PHYSICAL REVIEW D
PARTICLES AND FIELDS

THIRD SERIES, VOL. 6, NO. 1 — 1 July 1972

Positive-Pion Photoproduction in the Backward Direction*

K. Ekstrand,† A. Browman, L. Hand, and M. E. Nordberg, Jr.
Laboratory of Nuclear Studies, Cornell University, Ithaca, New York 14850
(Received 28 February 1972)

The reaction $\gamma + p \to \pi^+ + n$ has been measured for incident γ-ray energies from 0.7 to 8 GeV and recoil lab angles from 170° to 180° using the Cornell 10-GeV synchrotron. The data presented here cover the transition region between the resonance region and the high-energy region studied at SLAC. The results are compared with various phenomenological Regge-pole analyses and with similar data on π^0 photoproduction taken at DESY.

I. INTRODUCTION

Single-pion photoproduction at backward angles has been extensively studied in the low-energy resonance region up to a photon energy of 1.2 GeV.[1] Recent data on π^+ photoproduction at 180° in the resonance region has come from experiments done at Bonn University,[2] Tokyo University,[3] and Daresbury Nuclear Physics Laboratory.[4] In the high-energy region, where the Regge-pole analysis applies, the process has been studied at backward angles at SLAC.[5] The transition from the resonance region to the Regge region for π^0 photoproduction at 180° has been observed at DESY.[6] In this paper we report similar data for π^+.

It is convenient to analyze the process in terms of amplitudes corresponding to states of definite helicity. There are in general eight possible helicity amplitudes corresponding to an initial-state helicity of $\pm\frac{3}{2}$ and $\pm\frac{1}{2}$, and a final-state helicity of $\pm\frac{1}{2}$. Parity symmetry results in a relationship between states of opposite initial and final helicity[7] reducing the number of independent amplitudes to four. At 180° all but one of the independent amplitudes vanish since there is no orbital angular momentum and the spin of the initial state must be the same as that of the final state. For this reason it is quite natural to expect a drop in the cross section as the scattering angle approaches 180°. If, however, the dominant amplitude is the one which survives at 180° then there should be relatively little change in the cross section with angle.

The helicity arguments remain valid in the Regge-pole description. In this case the amplitudes are defined in terms of the u-channel scattering angle θ_u. Since $\cos\theta_u \to -1$ as $\cos\theta \to -1$ (θ being the center-of-mass scattering angle),[8] the vanishing of three out of the four amplitudes at 180° remains.

This experiment was performed using a bremsstrahlung beam from the Cornell 10-GeV electron synchrotron incident on a hydrogen target. A single wide-gap magnet along with a wire spark-chamber detection system was used to detect pions produced at laboratory angles between 170° and 180°. For each synchrotron energy setting the region between the maximum pion momentum for multiple-pion production and the maximum momentum for single-pion photoproduction is called the elastic region. It is in this momentum region that two-body kinematics are valid and the reaction is completely determined by the momentum and angle. Data for this experiment were taken primarily within the elastic region.

II. EXPERIMENTAL METHOD

A. General Considerations

Because the elastic momentum region became increasingly narrow as the synchrotron energy increased and because an uncertainty in pion momentum resulted in an increasingly large uncertainty in photon energy, the extension of this experiment into the high-photon-energy region required that the apparatus have good momentum resolution. At 180° every pion detected traveled through an indeterminant amount of target material and the momentum loss due to ionization necessitated that we limit our target length to 7.7 cm.

In order to achieve maximum beam we collimated it down very little, which led to a significantly large beam spot (diameter 1.9 cm). Since we could not treat the target as a point, for good momentum resolution a spark chamber was required within the magnet gap. The above considerations led to the general layout of scintillation counters, spark chambers, magnet, and hydrogen target as shown in Fig. 1. The spark chambers are labeled SC_1 to SC_7 while the scintillation counters are A, B, C_1 to C_3, L_1 to L_7 and K. The C and L counters provided a rough momentum analysis and this in coincidence with A, B, and K furnished the trigger for the spark chambers. The 2 in. of Lucite and the 2-in.-thick K scintillator absorbed most of the protons, which were produced in abundance through scattering from pole tips and other material in the target area.[9]

B. The Beam, Magnet, and Hydrogen Target

The beam was produced by bumping the circulating electron beam out of orbit onto a 1-mil copper target. The singles rates in counter A, which were only inches away from the beam line, were very sensitive to the collimation and this made the alignment of the beam collimators critical. After collimation the beam traveled in vacuum through a shielding wall and then through a channel which has been cut in the spectrometer magnet iron. After passing through the hydrogen target the beam continued in vacuum through a second wide-gap magnet. This was necessary since at 180° particles produced anywhere downstream from the target were indistinguishable from those produced at the target. The beam then passed through a secondary emission monitor and was stopped in a quantameter, which served as the primary beam monitor. The photon energy spectrum was calculated from the formulas tabulated by Koch and Motz.[10] The basic formulas were modified for the effect of target thickness and collimation angle by the calculation of Lutz and Schulz,[11] and for the absorption of photons by material in the beam line. The resultant spectrum was estimated to be accurate to within ±3%. The scattering chamber into which the cup was placed had a 10-mil Mylar window which produced a small but not negligible amount of multiple scattering of the pions.

The paths of charged particles of known momentum traveling through the field were determined by two methods. One consisted of integration of the track through the measured field distribution. The second method involved floating-wire measurements in the field. The floating-wire measurements were used primarily to determine a relationship between spark positions in the chambers and the momentum and production angle of the pions. The field integration was used to find the point of origin of the particle in the target plane.

C. Scintillation Counters and Spark Chambers

Counters A, the C's, and the L's were of conventional construction, consisting of plastic scintillator with Plexiglas light pipes and 2-in.-diameter photomultiplier tubes. A and the C's had long light pipes to bring the phototubes well out of the magnetic field. Because B and K were very long they had light pipes and phototubes on each end of the scintillator. The outputs from each end were summed by a passive resistance network.

The logic for the spark-chamber trigger was set so that only certain combinations of channels in the L and C hodoscopes produced triggers, pro-

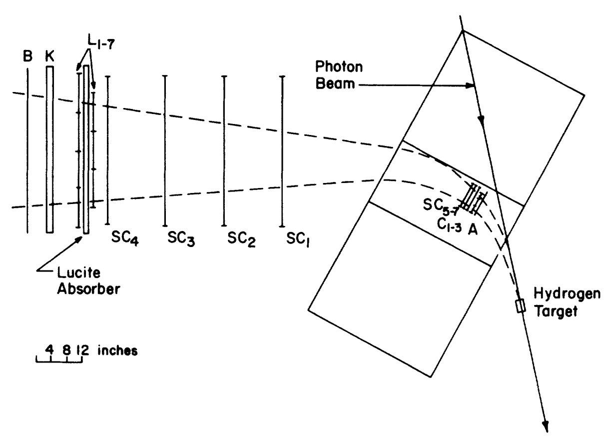

FIG. 1. The apparatus. Not shown are the primary and secondary collimators and magnetic sweeping upstream of the target in the photon beam, or the vacuum pipe and downstream sweeping magnet used to eliminate background from the beam stop.

viding an initial momentum analysis of the particles. For each event the time of flight between A and K was recorded. The time of flight provided a clean separation between pions and that small fraction of protons which penetrated the absorber.

The rear spark chambers, purchased from Science Accessories Corporation (SAC),[12] had an active area 24 in. vertically and 40 in. horizontally. The planes of chambers SC_5 to SC_7 were made of the same copper-nylon mesh as the SAC chambers. Because the magnetostrictive readout of these chambers was sensitive to magnetic fields it was necessary to extend the copper cloth beyond the spark-chamber frames, out of the magnet into a region of low field.

The information from the spark chambers, time of flight, and the hodoscopes were interfaced to an IBM 1800 computer by means of the Multiple Input Data Acquisition System of SAC. Much of the data analysis was at the same time as the data taking by the on-line computer.

III. ANALYSIS OF THE DATA

A. Track Finding and Momentum Analysis

In the first stage of analysis the output of the wire chambers was converted into spark positions which were compared with information from the L and C hodoscopes. Tracks were then calculated on the rear chambers with the requirement that in at least three out of four chambers a spark came within 0.5 cm of the track. From the track in the rear chambers and the point in the magnet chambers the momentum and production angle of the particle was determined. The path of the particle was then integrated back through the magnetic field to the target plane at which the point of origin of the particle was determined.

In the second stage of analysis cuts were placed on the data to reduce backgrounds and define the phase space. The first of these cuts, the time of flight cut, is illustrated in Fig. 2(a), which shows the time of flight distribution for a typical run along with the position of the cuts. At this point the data were cut to include only those events which fell within a well-defined solid angle and momentum region. Figure 2(b) shows the region of momentum and angle defined by the hodoscopes. Only events whose momentum and production angle fell within the large rectangle were included in further analysis. Next the data were cut on the difference between the position of the spark in the magnet chamber and the reconstructed track. This cut eliminated those pions which had undergone pole tip scattering in the magnet. The distribution of this difference along with the position of the cuts is shown in Fig. 2(c).

The final cut on the data was on the reconstructed position of origin of the particle at the target plane. Figure 2(d) shows the vertical distribution at the target plane. The position of the cuts was determined by calculating the expected distribution from the known beam spot size and by observing the momentum spectra for events within and outside the cuts. Both of these considerations indicated that the proper position of the cut is that indicated in Fig. 2(d). There was a considerable amount of background outside the cut. We therefore had to subtract a fraction of the events within the cut corresponding to this background. To do this we considered separately two types of events, those within the target cut, called inside-target events, and those immediately outside the cut in an equal area, called outside-target events. The outside-target events were subtracted from the inside-target events at the later stage of analysis.

B. Background Subtraction and Cross-Section Calculation

After all the cuts had been made the data for each run were binned according to pion momentum and in addition to the over-all momentum binning, we split up the 10° lab angular region into three equal regions and binned according to momentum and angle. Figure 3 shows the momentum spectra for runs at various synchrotron energy settings. The arrow indicates the expected cutoff due to the end point of the bremsstrahlung spectrum. The dotted line in each figure represents the amount of background which was expected from outside target and empty target momentum spectra. The solid line indicates the background that had to be subtracted in order to remove all the events from the kinematically forbidden region.

We will illustrate how the subtraction was arrived at by considering the example of 8.5 GeV where the subtraction was largest. Figure 4(a) shows the empty-target spectrum for this energy; Fig. 4(b) shows the spectrum for outside-target events. Both spectra could be represented by straight lines which when added together resulted in the known background. The additional subtraction which was the difference between the solid line and the dotted line was justified by the spectrum of π^- whose production was forbidden in the elastic π^+ momentum region. Figure 4(c) shows the observed π^- spectrum. The arrow indicates the threshold for π^- production. The counts which are in the region corresponding to the elastic region in the π^+ case are necessarily background. The solid line represents the background subtraction for the π^+ case discussed above. The fact that this represented a good background subtrac-

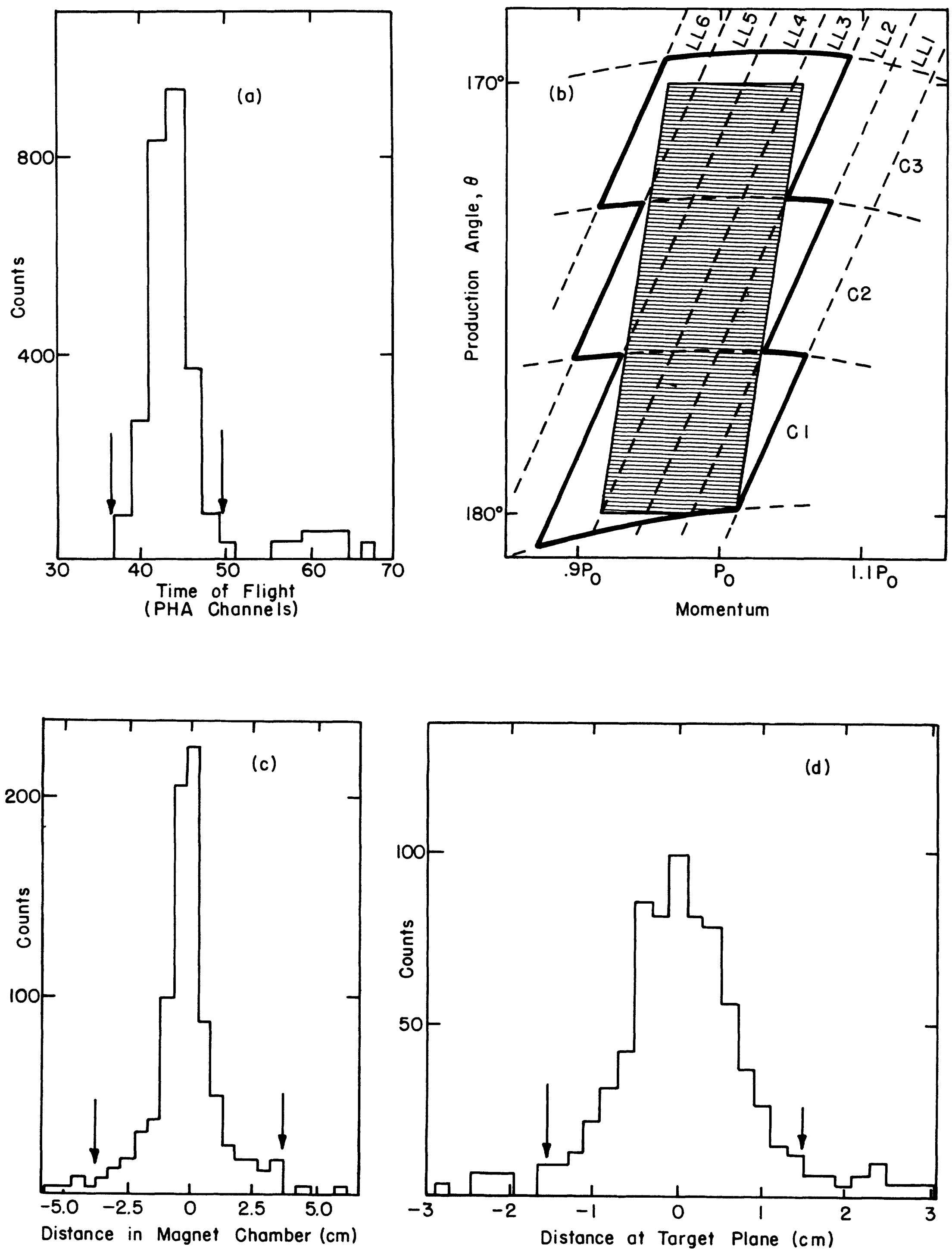

FIG. 2. (a) Time-of-flight spectrum, used primarily to separate pions from slower protons. (b) Momentum acceptance for a particular magnet setting. The heavy lines show the acceptance in P-θ for various counter combinations; the rectangle, the acceptance actually used for the data. (c) Correlation between measured position and calculated position for magnet spark chambers, assuming a point source. (d) Vertical distribution of trajectory intersections in a plane through the center of the target.

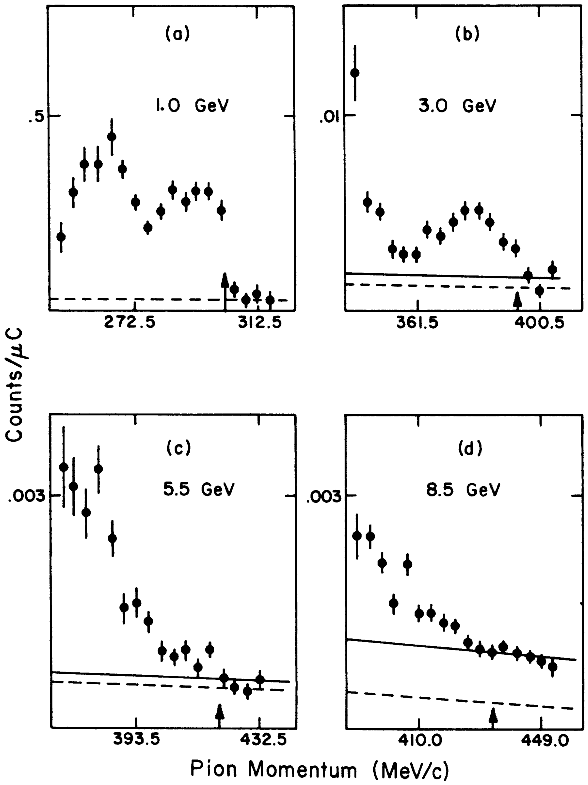

FIG. 3. Raw momentum spectra after prior cuts, before background subtraction. Energies shown are synchrotron energies.

tion for the π^- case gave us confidence in our subtraction procedure. An additional confirmation comes from the fact that the subtraction gives zero above the kinematic cutoff for the π^+ data.

The additional subtraction could be attributed to two effects, one of which is target frosting. It was observed that after the target had been cold for a long period of time, material had accumulated on the target walls which would greatly increase the empty-target background. The second effect lay in the outside-target subtraction. We assumed that the distribution of this background was the same within the beam spot as it was just outside the beam spot. It is more likely, however, that there was a greater amount of this type of background within the beam spot. Background from the illuminated target area has been observed in other experiments[5,13] and is generally attributed to double scattering processes.

The number of photons within each pion momentum bin was calculated by integrating the bremsstrahlung spectrum for our beam over the range of photon energies in the bin. In order to avoid difficulties due to uncertainties in the tip of the bremsstrahlung spectrum, only those bins whose maximum photon energy was below the synchrotron energy by 2% or more were considered in the calculation of the cross section. In addition to the cross section averaged over the entire angular region, the angular distribution was calculated from

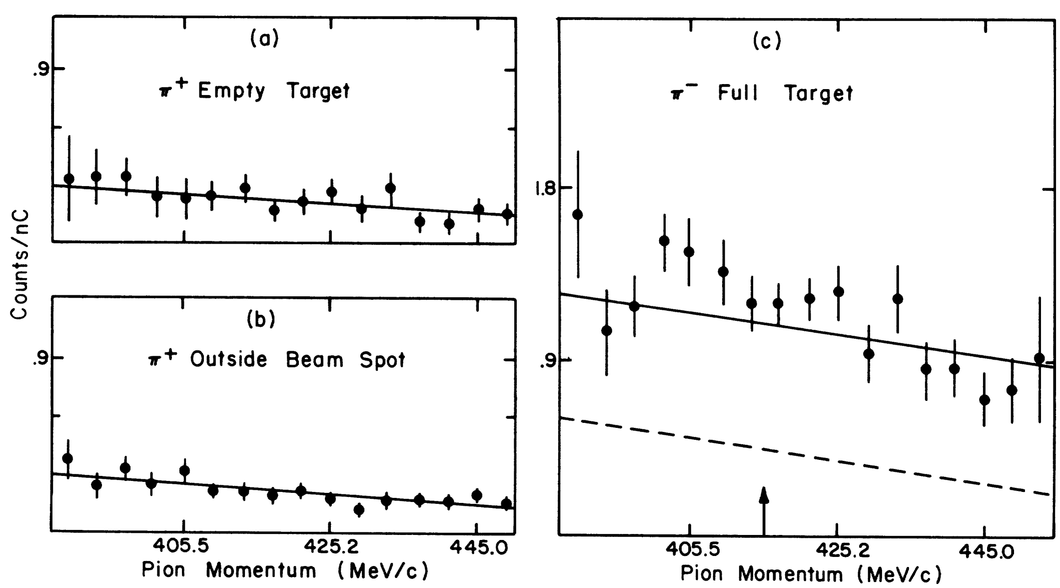

FIG. 4. (a) Empty-target background for π^+. (b) Spectrum of π^+ events outside vertical beam spot cuts. (c) π^- data contrasted with the sum of (a) and (b) from the π^+ data. All of the above correspond to 8.5 GeV and represent the worst case.

TABLE I. Tabulation of corrections in percent versus energy in GeV. For the first two entries the appropriate energy is photon energy. For the last three it is synchrotron energy. The percentage uncertainty due to this correction is below each entry in parentheses.

Correction \ Photon or synchrotron energy (GeV)	0.66	1	4	7
Decay in flight	21 (3.2)	17 (3.2)	12 (3.2)	12 (3.2)
Nuclear scattering	26 (4.9)	23 (4.3)	17 (2.8)	12 (2.8)
Quantametry		0 (0)	0 (0)	5 (2.5)
Dead time		2 (1)	9.6 (4.8)	12 (6)
Spark-chamber efficiency		1 (0.5)	8 (4)	6 (3)

the three 3.3° lab angle bins. From this the slope of the cross section, that is, the fractional rate of change of cross section with angle near 180° was calculated.

Data were taken with the synchrotron energy set at 1.0, 1.3, 1.75, 2.5, 3.0, 4.0, 4.2, 4.8, 5.5, 6.4, and 8.5 GeV. At adjacent energy settings there was an overlap in the elastic momentum regions. The data within a small region of photon energy were combined by a weighted least-squares fit assuming a linear variation of cross section with energy.

C. Errors and Corrections

The momentum resolution of the system was determined primarily by multiple scattering of the pion. The momentum loss as the pion traveled through the target material resulted in a momentum uncertainty of 0.43% at the pion momentum of 300 MeV/c, corresponding to a 1-GeV photon. The scattering of pions in the detection system resulted in a momentum uncertainty of 0.51%. The resultant momentum resolution was ±0.68%. The effect of this momentum resolution was to smear the edge of the bremsstrahlung cutoff at 1 GeV, resulting in an uncertainty in the photon energy determination which varied from 0.9% at 1 GeV to 5% at 7 GeV.

The loss of events due to decay of the pion in flight was determined taking into account those decays in which the flight of the muon resulted in a good event. The loss of events due to nuclear scattering was calculated using the data of Petrov *et al.*,[14] who measured the scattering of pions from carbon and lithium in the kinetic-energy region at 200 MeV.

The only counters which had significant dead-time corrections were A, B, K, and the C's. The total correction was the product of the individual corrections except for that of the C's for which the correction was reduced by $\frac{1}{3}$ since they are independent counters and were counting at approximately the same rate.

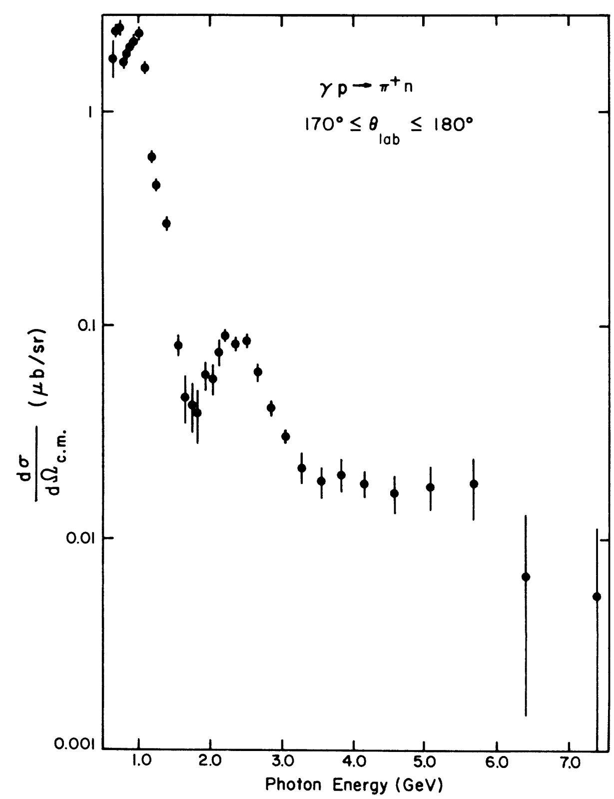

FIG. 5. Center-of-mass cross section averaged over 10° laboratory angular region vs photon energy.

TABLE II. Values of the 10° average center-of-mass cross section, the slope of the cross section with center of mass angle, and the 180° cross section.

Photon energy (GeV)	$\left(\frac{d\sigma}{d\Omega}\right)_{c.m.}$ 10° av (μb/sr)	Error	$\Delta\left(\frac{d\sigma}{d\Omega}\right)\Big/\frac{d\sigma}{d\Omega}\,\Delta\theta_{c.m.}$ (rad)	Error	$\left(\frac{d\sigma}{d\Omega}\right)_{c.m.}$ 180° (μb/sr)	Error
0.66	1.84	0.31	−10.5	4.7	2.64	0.40
0.69	2.35	0.25	−4.76	3.2	3.16	0.38
0.74	2.45	0.21	−5.47	3.2	3.02	0.34
0.78	1.76	0.10	−2.83	1.5	2.08	0.17
0.84	1.90	0.11	−5.16	1.8	2.10	0.18
0.90	2.04	0.094	1.41	1.5	2.04	0.18
0.96	2.14	0.100	−2.62	1.5	1.93	0.19
1.03	2.26	0.11	1.79	1.7	1.94	0.19
1.11	1.61	0.082	5.24	1.6	1.22	0.14
1.22	0.658	0.028	5.70	1.4	0.480	0.052
1.31	0.456	0.027	6.58	2.0	0.316	0.049
1.45	0.300	0.017	4.62	1.7	0.199	0.031
1.60	0.0825	0.012	11.6	2.8	0.0538	0.014
1.70	0.0449	0.014	4.77	3.4	0.0306	0.015
1.77	0.0411	0.013	8.36	3.6	0.0282	0.014
1.86	0.0386	0.013	4.50	3.1	0.0283	0.014
1.94	0.0565	0.010	6.30	2.8	0.0449	0.011
2.05	0.0549	0.0097	6.58	2.4	0.0470	0.011
2.16	0.0755	0.0100	−0.18	2.3	0.0701	0.011
2.27	0.0900	0.0070	2.87	1.9	0.0815	0.0094
2.40	0.0806	0.0064	8.35	1.6	0.0655	0.0084
2.54	0.0805	0.0059	5.05	1.6	0.0641	0.0075
2.69	0.0598	0.0052	7.98	1.7	0.0470	0.0060
2.87	0.0429	0.0043	5.02	1.7	0.0347	0.0047
3.09	0.0298	0.0042	7.38	1.9	0.0242	0.0044
3.31	0.0225	0.0035	6.11	1.9	0.0185	0.0036
3.57	0.0184	0.0030	4.63	1.8	0.0157	0.0032
3.86	0.0202	0.0037	−1.15	2.3	0.0179	0.0039
4.20	0.0181	0.0039	3.55	2.5	0.0164	0.0040
4.65	0.0167	0.0035	7.12	2.6	0.0158	0.0037
5.12	0.0174	0.0042	−0.071	2.8	0.0168	0.0044
5.71	0.0178	0.0059	3.99	3.5	0.0174	0.0060
6.45	0.0066	0.0062	−6.45	5.5	0.0065	0.0062
7.38	0.0054	0.0057	6.45	5.9	0.0056	0.0057

The total spark-chamber efficiency correction was determined by multiplying the separate corrections due to the rear and magnet chamber systems. The efficiency of the chamber systems was determined by calculating the probability for a track being missed from the efficiency of the individual chambers. The rates at which the individual chambers failed were compiled on line by the computer and the efficiency corrections were determined at the end of the runs. This procedure neglects correlated losses, but assuming these would be rate dependent, a check can be made by observing the consistency of data taken at different rates.

In addition to the corrections discussed above there was an energy-dependent correction due to losses in the quantameter, the effect of which has been measured by Loe.[15] The above corrections varied in general with energy, photon energy for the case of decay in flight and nuclear scattering and synchrotron energy for the case of dead time, quantametry and spark-chamber efficiency. Table I lists the corrections in per cent at a number of energies as well as the percentage uncertainty in the cross section due to this correction. In addition to these uncertainties there were energy-independent uncertainties in the target length, 1%, solid angle, 3%, and bremsstrahlung spectrum, 3%. The primary uncertainties in the data were due to counting statistics and the background subtraction. The uncertainty in the background subtraction was taken to be the standard error in the

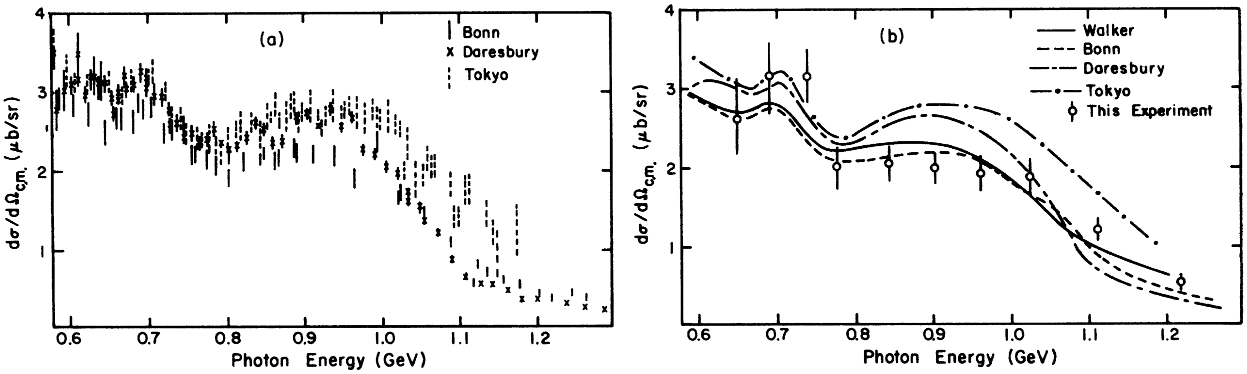

FIG. 6. (a) Bonn, Tokyo, and Daresbury data plotted together showing disagreement at low energies (Refs. 2–4). (b) Same, with data from this experiment in the same energy region. These are 180° cross sections.

least-squares fit to the outside target and empty-target spectra plus half the additional subtraction.

IV. RESULTS AND CONCLUSIONS

A. Comparison with Previous Measurements

Figure 5 shows the center-of-mass cross section which we measured over the 10° laboratory angular region as a function of photon energy. The error bars represent statistical errors, uncertainties from the background subtraction, and energy dependent uncertainties discussed above. A 5.4% systematic uncertainty is not included. Table II lists the cross section in this figure, the slope of the cross section, that is, the fractional rate of change of cross section with center-of-mass angle, and the cross section extrapolated to 180° using the value of the slope obtained from a smooth curve through the values at each energy.

Although the primary thrust of this experiment lay in the measurement of the cross section in the intermediate energy region, comparison with lower-energy data provided a check for our higher-energy data. Figure 6(a) shows the Bonn, Tokyo,

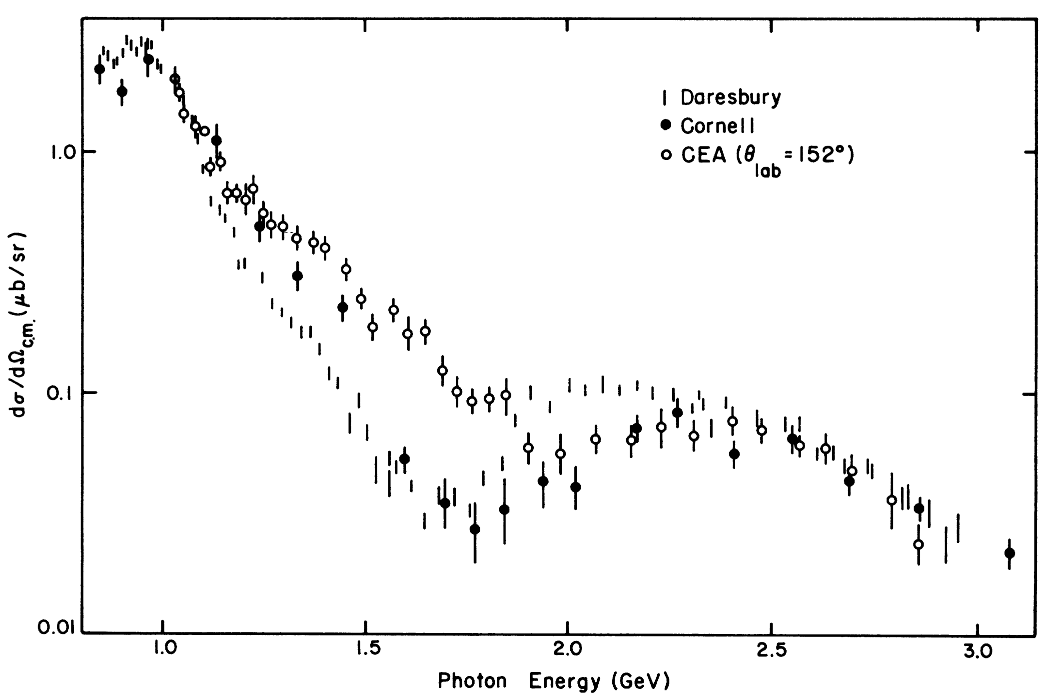

FIG. 7. A comparison of data from this experiment with Daresbury data, also at 180°, and CEA data (Ref. 13) at 152°.

and Daresbury data plotted together. Smooth curves corresponding to these data are depicted in Fig. 6(b) along with our 180° data and the prediction of the analysis of Walker. Unfortunately our data do not have enough statistics to decide among the three measurements.

Figure 7 presents our data along with the Daresbury data over the energy range from 0.8 to 3 GeV. Included in the diagram are the data of Alvarez *et al.*,[13] measured at a laboratory angle of 152°. The disagreement between our data and the Daresbury data in the region between 1.1 to 1.5 GeV is not too severe since the cross section is dropping rapidly and a shift in the energy scale of one experiment relative to the other by 6% will bring the data into agreement. A more serious discrepancy lies in the energy region between 1.8 and 2.3 GeV. The Daresbury data lie above not only our data but also the 152° (laboratory angle) CEA data. As was stated previously, the vanishing of three out of four of the helicity amplitudes implies that an increase in the cross section with angle at 180°, as is implied by the Daresbury data along with the CEA data at 2 GeV, is unlikely.

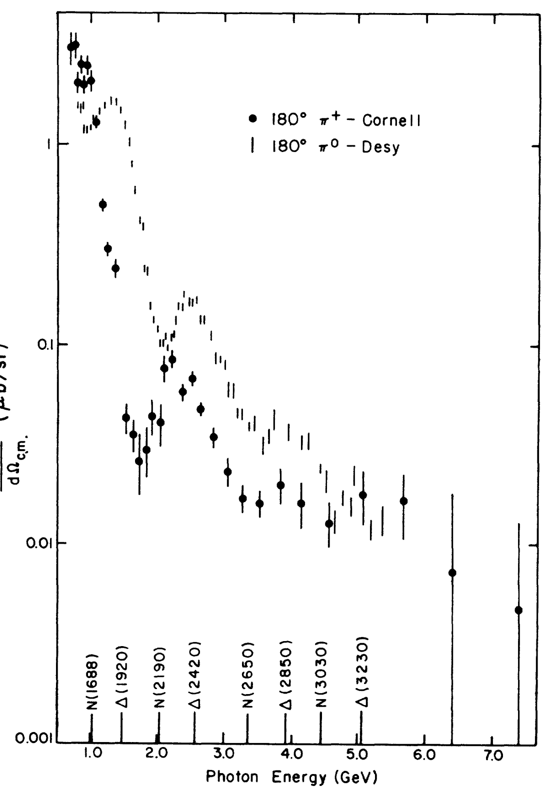

FIG. 8. A comparison of this data for 180° π^+ photoproduction with the DESY data for 180° π^0 production in the same energy region.

Figure 8 illustrates the comparison of our 180° π^+ data with the π^0 data of DESY. The difference between the energy dependence of the two reactions is striking. The positions of the well-known πP resonances are indicated in the diagram. There appears to be a tendency for π^+ to favor the N resonances and π^0 to favor the Δ's.

B. Comparison with Existing Theories

Figure 9 shows the angular distributions of our data at 2.8 and 5 GeV along with some of the data at smaller angles from SLAC and CEA. The Cornell 2.8-GeV data is compiled from our data at photon energies from 2.7 to 2.9 GeV, while the 5-GeV data are averaged between 4.2 and 5.7 GeV. The data are compared with various Regge theories. At 5 GeV the simple Regge pole theories of Barger and Weiler,[16] Beaupre and Paschos,[8] and Bajpaj[17] are all essentially in agreement with the data. The fit of Kelly, Kane, and Henyey,[18] which employs Regge cuts, predicts a much steeper drop in the cross section at 180° than is seen in our data. The 2.8-GeV angular distributions are compared with those of Barger and Weiler and of Bajpaj. Neither results in a very good agreement with our data. This is not surprising since at this energy we are near a resonance and the Regge-pole theory does not apply in detail here. The

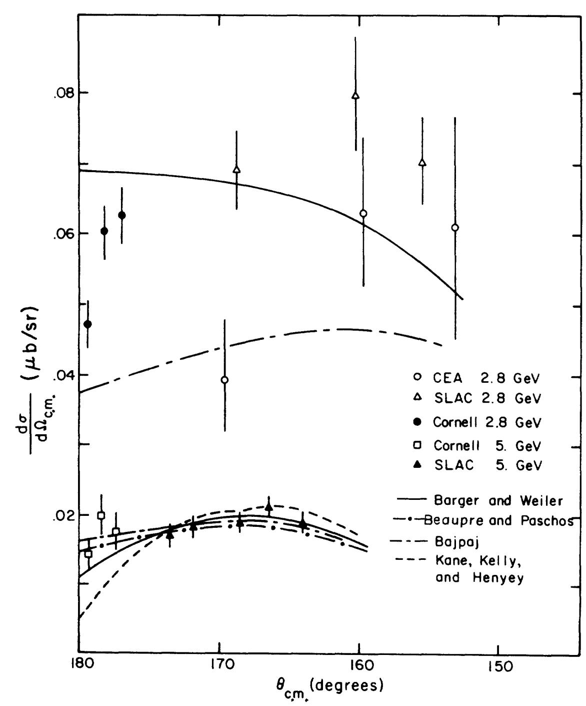

FIG. 9. Angular distribution at 2.8 and 5 GeV compared to SLAC and CEA data at smaller angles and to various theoretical fits.

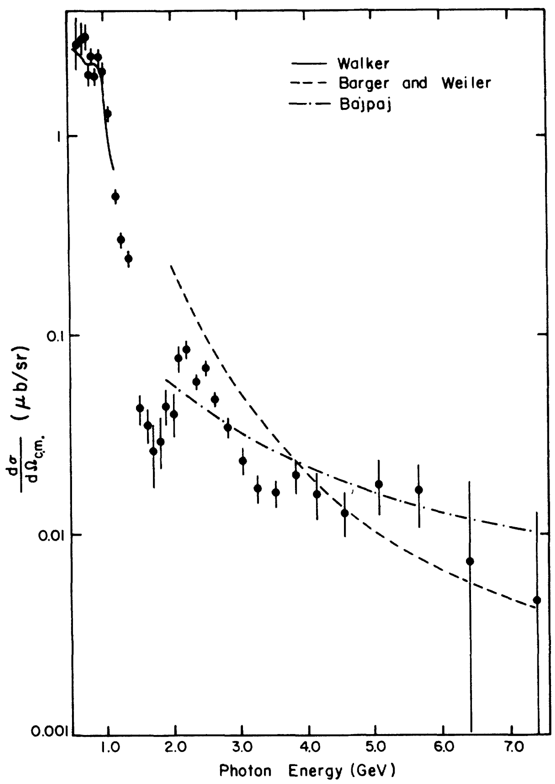

FIG. 10. Energy dependence of the π^+ cross section at 180° compared with the theoretical fits.

duality between s-channel resonances and u-channel Regge exchanges implies that the Regge fits should pass through the average of the cross section in the resonance region.[19] Figure 10 shows the energy dependence of our 180° cross section along with the low-energy Walker fit and the predictions of Barger and Weiler and of Bajpaj. In this case only the fit of Bajpaj is in good agreement with our data.

C. Inelastic Data

At the synchrotron energies of 3 and 8.5 GeV, data were taken inside the inelastic region in order to get some idea of the magnitude of inelastic production. Having measured the elastic cross section over the entire photon energy range, we determined the expected number of counts from elastic events and, by subtraction, arrived at the purely inelastic backward pion momentum spectrum. At 3 GeV no inelastic production could be seen over the entire momentum range studied, which extended from the elastic threshold, 393 MeV/c, down to 320 MeV/c. The threshold for inelastic production at 3 GeV is 373 MeV/c and Δ(1236) production has a threshold at 345 MeV/c.

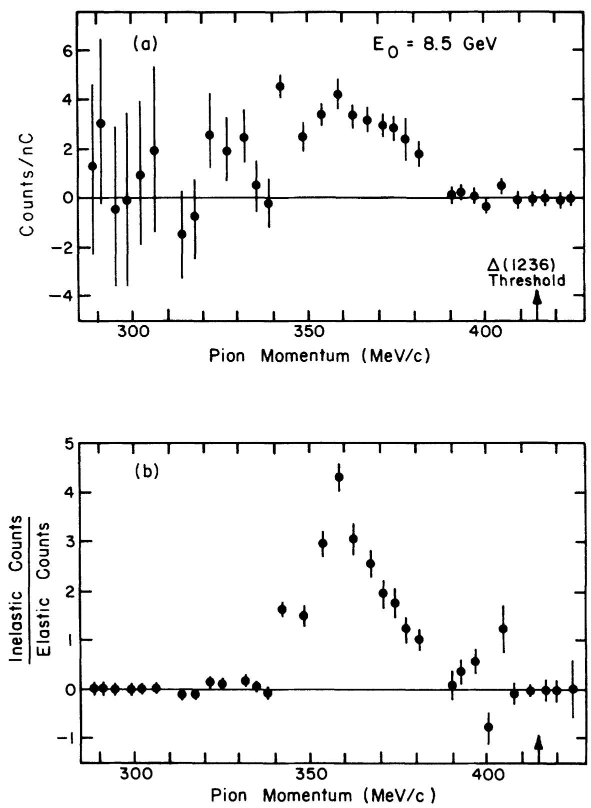

FIG. 11. (a) Yield of backward π^+ with measured elastic yields subtracted. (b) Ratio of total number of backward π^+ to the number of elastic π^+.

The upper limit for inelastic production was 20% of the elastic production over the entire momentum range. At 8.5-GeV synchrotron energy some inelastic events were observed, as is indicated in Fig. 11(a), which shows the backward pion yield with the elastic yield subtracted off, and in Fig. 11(b), which shows the ratio of inelastic to elastic yields. The arrow in the figure shows the threshold for Δ(1236) production. At other synchrotron energy settings some data were taken in the inelastic region down to the Δ(1236) threshold. The result was that no inelastic events could be seen below 5 GeV and inelastic events were visible above 5 GeV.

The absence of inelastic production at 180° at low photon energy has also been seen in π^-p scattering in Anthony *et al.*,[20] who compared elastic π^-p scattering with Δ(1236) production at 2.15 GeV, finding π^- production at smaller angles but not at 180°. The abrupt appearance of inelastically produced pions at 5 GeV is surprising. If this is due to the threshold excitation of a resonance, then the mass of the resonance is on the order of 3000 MeV. In any case, it appears that inelastic pion photoproduction at 180° is an interesting area for further study.

We would like to thank the operating crew of the Cornell 10-GeV machine for supplying a beam of excellent quality throughout the data-taking phase of the experiment. R. Helmke performed a major service both with the time-sharing software for the IBM 1800 computer and with an assembly language routine for the magnet integration which considerably improved the analysis time. A. Loomis helped with the early stages of the experiment.

---

*Work supported by the National Science Foundation.

†Present address: Laboratori Nazionali di Frascati, Italy.

[1]A summary of the data up to 1969 along with a phenomenological analysis appears in a paper by R. L. Walker, Phys. Rev. 182, 1729 (1969).

[2]G. Fischer *et al.*, paper submitted to the Fifteenth International Conference on High-Energy Physics, Kiev, U.S.S.R., 1970 (unpublished).

[3]T. Fujii *et al.*, paper submitted to the Fifteenth International Conference on High-Energy Physics, Kiev, U.S.S.R., 1970 (unpublished).

[4]B. D'Almague, thesis, l'Université de Paris, Centre d'Orsay, 1970 (unpublished).

[5]R. L. Anderson *et al.*, Phys. Rev. Letters 23, 725 (1969); see also 21, 479 (1968).

[6]G. Buschorn *et al.*, Phys. Rev. Letters 20, 230 (1968).

[7]M. Jacob and G. C. Wick, Ann. Phys. (N.Y.) 7, 404 (1959).

[8]J. V. Beaupre and E. A. Paschos, Phys. Rev. D 1, 2040 (1970).

[9]A detailed discussion of the apparatus and experimental method is contained in K. Ekstrand, Ph.D. thesis, Cornell University, 1971 (unpublished).

[10]H. W. Koch and J. W. Motz, Rev. Mod. Phys. 31, 920 (1959).

[11]G. Lutz and H. D. Schulz, DESY Report No. 67/29, 1967 (unpublished).

[12]Science Accessories Corporation, 65 Station Street, Southport, Conn.

[13]R. Alvarez *et al.*, Phys. Rev. D 1, 1946 (1970).

[14]N. I. Petrov *et al.*, Zh. Eksp. Teor. Fiz. 37, 957 (1959) [Sov. Phys. JETP 10, 682 (1960)]; V. G. Ivonov *et al.*, *ibid.* 37, 863 (1959) [*ibid.* 10, 615 (1960)]; V. T. Osipenkov and S. S. Filipov, *ibid.* 34, 224 (1958) [*ibid.* 7, 154 (1958)].

[15]R. Loe (private communciation).

[16]V. Barger and P. Weiler, Phys. Letters 30B, 105 (1969).

[17]R. D. Bajpaj, Lett. Nuovo Cimento 4, 950 (1970).

[18]R. L. Kelly, G. L. Kane, and F. Henyey, Phys. Rev. Letters 24, 1511 (1970).

[19]R. Dolen, D. Horn, and C. Schmid, Phys. Rev. 166, 1768 (1968).

[20]R. Anthony *et al.*, Phys. Rev. Letters 21, 1605 (1968).

PHYSICAL REVIEW D VOLUME 6, NUMBER 1 1 JULY 1972

Interference Effects of $K^*(890)$ and $K^*(1420)$ Resonances with the Background*

M. Aguilar-Benitez, S. U. Chung, and R. L. Eisner
Brookhaven National Laboratory, Upton, New York 11973
(Received 22 February 1972)

We have made a study of interference effects between $K^*(890)$ and $K^*(1420)$ resonances and the background as observed in the reaction $K^-p \rightarrow K^-\pi^+n$ at 3.9- and 4.6-GeV/c incident momenta, using a mass-dependent formalism which utilizes the generalized multipole moments. From this analysis we have obtained the $K^*(890)$ and $K^*(1420)$ density-matrix elements in the Jackson frame which satisfy the spin-1 and spin-2 positivity conditions, respectively. We discuss the implications of the degree and the phase of the interference on the nature of the production mechanism as well as the question of whether there exists a daughter resonance near the $K^*(1420)$.

I. INTRODUCTION

The purpose of this paper is to study interference effects between $K^*(890)$ and $K^*(1420)$ resonances and the background. Particular emphasis has been given to the problem of extracting density-matrix elements $\rho_{mm'}$ when the resonance interferes with the background.

This study has been motivated by the long-standing problem[1-3] that one of the diagonal density-matrix elements (i.e., ρ_{22}) for spin-2 resonances such as $f^0(1250)$ or $K^*(1420)$ is found to be nega-